Temperature-dependent study reveals that dynamics of hydrophobic residues plays an important functional role in the mitochondrial Tim9-Tim10 complex

ARTICLE *in* PROTEINS STRUCTURE FUNCTION AND BIOINFORMATICS · FEBRUARY 2012

Impact Factor: 2.63 · DOI: 10.1002/prot.23224 · Source: PubMed

7 AUTHORS, INCLUDING:

Jiayun Pang
University of Greenwich
23 PUBLICATIONS **357** CITATIONS
SEE PROFILE

Thomas A Jowitt
The University of Manchester
57 PUBLICATIONS **904** CITATIONS
SEE PROFILE

Guanhua Yan
The University of Manchester
3 PUBLICATIONS **28** CITATIONS
SEE PROFILE

Hui Lu
The University of Manchester
28 PUBLICATIONS **1,806** CITATIONS
SEE PROFILE

PROTEINS
STRUCTURE ■ FUNCTION ■ BIOINFORMATICS

Temperature-dependent study reveals that dynamics of hydrophobic residues plays an important functional role in the mitochondrial Tim9–Tim10 complex

Ekaterina Ivanova,[1,2]† Jiayun Pang,[1,3]† Thomas A. Jowitt,[2] Guanhua Yan,[2] Jim Warwicker,[1,2] Michael J. Sutcliffe,[1,3] and Hui Lu[1,2]*

[1] Manchester Interdisciplinary Biocentre, University of Manchester, Manchester M1 7DN, United Kingdom
[2] Faculty of Life Sciences, University of Manchester, Oxford Road, Manchester M13 9PT, United Kingdom
[3] School of Chemical Engineering and Analytical Science, University of Manchester, Oxford Road, Manchester M13 9PL, United Kingdom

ABSTRACT

Protein–protein interaction is a fundamental process in all major biological processes. The hexameric Tim9–Tim10 (translocase of inner membrane) complex of the mitochondrial intermembrane space plays an essential chaperone-like role during import of mitochondrial membrane proteins. However, little is known about the functional mechanism of the complex because the interaction is weak and transient. This study investigates how electrostatic and hydrophobic interactions affect the conformation and function of the complex at physiological temperatures, using both experimental and computational methods. The results suggest that, first, different complex conformational states exist at equilibrium, and the major difference between these states is the degree of hydrophobic interactions. Second, the conformational change mimics the biological activity of the complex as measured by substrate binding at the same temperatures. Finally, molecular dynamics simulation and detailed energy decomposition analysis provided supporting evidence at the atomic level for the presence of an excited state of the complex, the formation of which is largely driven by the disruption of hydrophobic interactions. Taken together, this study indicates that the dynamics of the hydrophobic residues plays an important role in regulating the function of the Tim9–Tim10 complex.

Proteins 2012; 80:602–615.

Key words: protein–protein interaction; hydrophobic effect; stopped-flow; kinetics; simulation.

INTRODUCTION

Structure and dynamics play crucial roles in protein function.[1–3] For many proteins, biological functions depend on molecular dynamics (MD), which can lead from highly populated ground states (G state) to low-populated excited states (E state) that are functionally important. However, little is known about the structures of excited states and the links between protein dynamics and function, because the low population and transient nature of such states make them undetectable by conventional structural techniques. The complex formed by Tim9 and Tim10 (translocase of inner membrane) proteins of the mitochondrial intermembrane space (IMS) plays an essential chaperone-like role during the import of mitochondrial membrane proteins, probably by interacting with them transiently and preventing aggregation of the hydrophobic proteins in the aqueous environment of the IMS.[4–6] Unlike classic chaperones, such as Hsp70s and Hsp60s, the hexameric Tim9–Tim10 complex ($\alpha_3\beta_3$) belongs to a novel chaperone family, whose function is ATP independent. Although substrate capture and release by the classic chaperones is regulated by ATP hydrolysis,[7,8] how ATP-independent chaperones bind and release their substrates remains unknown.

Both Tim9 and Tim10 are members of an evolutionarily conserved "small Tim" family, which contain a strictly conserved $CX_3C–X_n–CX_3C$ (n = 15/16, C = Cys) motif. Both proteins are folded in a molten-globule-like state, with loosely packed α-helical structure.[9,10] Sedimentation equilibrium studies showed that although Tim9 forms a homodimer, Tim10 is a monomer.[11] Intramolecular disulphide bond formation is

Additional Supporting Information may be found in the online version of this article.
Abbreviations: CD, circular dichroism; IMS, intermembrane space; RMSDs, root-mean-square deviations; RMSFs, root-mean-square fluctuations; Tim, translocase of inner membrane.

Grant sponsor: Royal Society; Grant sponsor: the Leverhulme Trust; Grant number: F/00120/CB; Grant sponsor: Biotechnology and Biological Sciences Research Council; Grant numbers: BB/C514323 and BB/H017208.
†The authors contribute equally to the work.
*Correspondence to: Hui Lu, Manchester Interdisciplinary Biocentre, University of Manchester, 131 Princess Street, Manchester M1 7DN, United Kingdom. E-mail: hui.lu@manchester.ac.uk
Received 26 May 2011; Revised 20 September 2011; Accepted 12 October 2011
Published online 19 October 2011 in Wiley Online Library (wileyonlinelibrary.com).
DOI: 10.1002/prot.23224

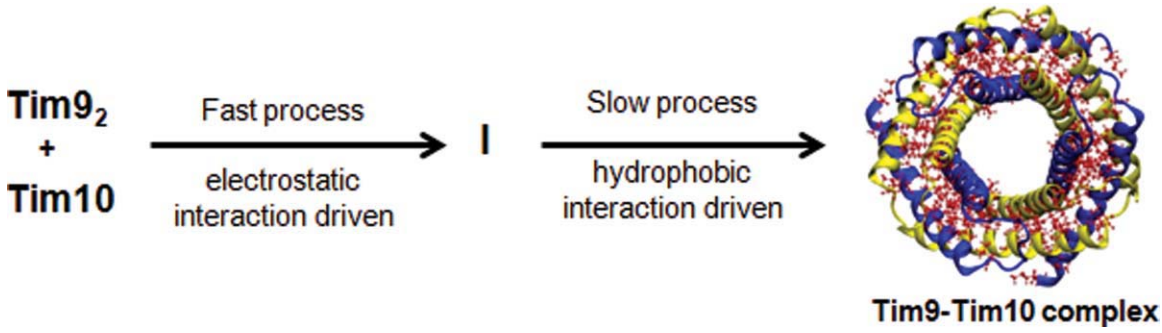

Figure 1

An assembly pathway of the Tim9–Tim10 complex.[11,15] The complex is formed in a multikinetic process with the formation of assembly intermediates (I) and the reaction can be divided into two major processes. While the fast process is driven by electrostatic protein–protein interactions, the slow process is dominated by hydrophobic interactions. The crystal structure of the Tim9–Tim10 complex (Protein Data Bank id: 3DXR) is shown with Tim9 in yellow, Tim10 in blue, and side chain of hydrophobic residues are shown in red. [Color figure can be viewed in the online issue, which is available at wileyonlinelibrary.com.]

essential for folding of Tim9, Tim10, and formation of the Tim9–Tim10 complex.[10,12] The crystal structure of the Tim9–Tim10 complex shows an α-propeller topology with three Tim9 and three Tim10 subunits arranged alternately, giving a central ring-shaped structure with a double layer (Fig. 1).[13,14] Both subunits fold in a helix–loop–helix structure in the complex, featured by two extended and tentacle-like N- and C-terminal helices. The six N-terminal helices together form the inner layer and the six C-terminal helices together form the outer layer of the ring-shaped structure. Interestingly, most of the hydrophobic residues of the subunits are buried between the two layers. There is not an obvious hydrophobic pocket for substrate binding, suggesting that a conformational change is required for substrate binding by the Tim9–Tim10 complex.

The kinetics of the Tim9–Tim10 complex formation was characterized using stopped-flow fluorescence and stopped-flow light scattering techniques.[11,15] In previous studies, a set of single Trp mutants, with the intrinsic fluorescence probe located in N- and C-terminal helices and the central loop regions, were used to decipher the kinetic process of assembly. We have shown that the complex formation is a multistep process with formation of assembly intermediates (Fig. 1). The N-terminal helices of both subunits are assembled faster than the C-terminal helices.[11] More importantly, pH-dependent and salt effect studies reveal that the fast association process is driven by electrostatic protein–protein interactions, whereas the slow process is dominated by hydrophobic interactions.[15] Thus, the major hydrophobic areas located between the N- and C-terminal helices may be less protected or loosely packed in the assembly intermediates, which may more accessible to substrate binding. Although interesting kinetic intermediates were observed, whether such a state or different conformational states of the complex exist at equilibrium under a steady state condition is unknown.

The aim of this study is to investigate whether different conformational states or a low-populated exited E state of the Tim9–Tim10 complex exist at equilibrium and their possible roles in the function of the complex. Because the conformational difference is small and subtle, a very sensitive analysis is required. To this end, we used stopped-flow fluorescence coupled with temperature-dependent analysis to investigate whether/how electrostatic and hydrophobic protein–protein interactions change with mild temperature increase, and their correlation with the structure and function (substrate binding properties) of the Tim9–Tim10 complex. First, thermal denaturation of the complex was studied, which showed that the complex is stable at temperatures below 45°C and has a melting temperature at 52°C. Next, the kinetics of the complex formation was studied at temperatures below 45°C. We show that although the rate of the fast process (driven by electrostatic protein–protein interactions) increased exponentially with temperature according to the Arrhenius equation, the slow process did not. A bell-shaped temperature-dependent curve was obtained for the slow process (hydrophobic interactions), with an inflection point at about 25–30°C. The result shows that there is a heat capacity and thus a conformational change in the Tim9–Tim10 complex, suggesting the presence of a low-populated excited state at physiological temperatures. Third, we showed that the bell-shaped curve of the complex mimics the biological activity of the Tim9– Tim10 complex as measured by substrate binding. Finally, MD simulations and detailed energy decomposition analysis provided evidence at the atomic level for the presence of an excited state, and its formation being driven by disruption of the hydrophobic interactions. Taken together, using experimental and computational methods (a bottom-up approach), we showed that the dynamics of the hydrophobic interactions play an important role in regulating the function of the ATP-independent chaperone Tim9–Tim10 complex.

MATERIALS AND METHODS

Protein purification

All the wild type and mutant proteins were expressed in *Escherichia coli* Rosetta-gami™ 2 cells (Novagen) as a GST-Tim fusion protein using pGEX 4T-1 vector (GE Healthcare). Each protein was purified using GST affinity beads followed by fusion cleavage with thrombin and gel filtration using FPLC superdex 75 as described previously.[11] All experiments were carried out in 150 m*M* NaCl, 50 m*M* Tris–HCl buffer pH7.4, unless stated otherwise.

Stopped-flow fluorescence measurements

Stopped-flow fluorescence measurements were performed using the SX.18MV-R stopped-flow reaction analyzer from Applied PhotoPhysics. The assembly reaction was initiated by rapid mixing of two proteins at the same concentration (between 5 and 20 μM) and a ratio of 1:1 (v/v). The mixing dead time was less than 2 ms. Time course of the complex formation was measured by following Trp fluorescence intensity change using an excitation wavelength of 295 nm and a cut off filter of 305 nm for the mutants, and an excitation wavelength of 275 nm and a cut off filter of 295 nm for Tyr of the wild type proteins. Each reaction curve represents an average of at least three experimental runs depending on the sensitivity of the fluorescence signals. The overall rate constant for the fast or slow process of the complex formation was analyzed using a single exponential function $F(t) = F_0 + A(\exp(-k_{obs}t))$, or $F(t) = F_0 + A(\exp(-k_{obs}t)) + Bt$, where A is amplitude, k_{obs} is the observed rate constant, and B is constant. The data analysis was produced using the software Origin 6.0 and Sigma Plot 7.0. For the peptide binding experiments, Tim9–Tim10 complex was mixed with the peptide derived from the third transmembrane fragment of ADP/ATP carrier (AAC; TM3, KKYAKWFAGNLASGGAAG ALSLLFVYSLY) at a molar ratio of 1:1.

Circular dichroism measurements

Circular dichroism (CD) analysis was performed using a JASCO J810 spectropolarimeter with a 1-3mm path-length quartz cuvette. Far-ultraviolet (UV) CD spectra were measured at 20°C with 300 μL complexes (typically 0.1 mg/mL) as described previously.[16] Each spectrum represents an average of four scans from 200 to 260 nm at 0.2 nm intervals with the spectra for buffer alone subtracted.

Thermal denaturation

Thermal denaturation was studied by following CD intensity at 222 nm, at 1°C/min over temperature of 5–90°C as described previously.[17] It is also studied by following Tyr or Trp fluorescence intensity change. The excitation and emission wavelengths of 275 and 303 nm were used for Tyr. The excitation wavelength of 295 and emission at 320 or 350 nm were used for the Trp mutants.

Biacore measurements

All the experiments were carried out using 50 m*M* Tris pH 7.4, 150 m*M* NaCl, and 0.05% Nonidet P20 with a flow rate of 40 μL/min. The temperature dependence of complex formation between Tim9 and Tim10 was performed using the thermodynamics program on a Biacore T100. Approximately 400 units of Tim10 were immobilized on the surface of a CM5 chip using the EDC/NHS activation of carboxyl groups followed by two blocking cycles of ethanolamine at 10 μL/min. At each temperature of 12, 20, 25, 30, 37, and 43°C, 100 n*M* of Tim9 in a running buffer was injected for binding with Tim10. Tim10 was regenerated with a 60 s pulse of acetate buffer at pH 4.5 after each measurement. The interactions between Tim9–Tim10 complex and peptide TM3 were studied using a Biacore 3000 instrument. Approximately 200 units of N-terminal biotin labeled TM3 (Biotin-KKYAKWFAGNLASGGAAGALSLLF-VYSLDY) was immobilized on a Biacore SA chip at 10 μL/min. A 67-nM Tim9–Tim10 complex was used for the binding studies at each temperature with a flow rate of 40 μL/min. Regeneration of the peptide was performed using a 30 s pulse of 4 M GuHCl. All experiments were repeated three times and double referenced with the buffer alone. The data were analyzed using the initial rate method as described in the text using the software Origin 6.0 and Sigma Plot 7.0.

MD simulations

MD simulations were performed at 300 K, 400 K, and 450 K using AMBER9[18] with AMBER ff03 force field[19] and a generalized Born (GB) solvent model.[20] Initial protein coordinates were taken from the crystal structure of the Tim9–Tim10 complex (3DXR.pdb).[14] The final structure contains 414 residues in the hexamer with 138 residues in each pair of Tim9 and Tim10 (69 in Tim9 and 69 in Tim10). Hydrogen atoms were added using the Leap program within the AMBER package. Following initial energy minimization, the system was heated from 0 to 300 K, 400 K, and 450 K, respectively, and equilibrated for 20 ps. The final production trajectory was collected for 1 ns. The nonbonded cutoff was set to 999 Å. Bonds to hydrogen atoms were constrained using the SHAKE algorithm. A time step of 0.002 ps was used, and the coordinates were saved every 1 ps.

Free energy calculations

The MM-PB/GBSA is an approach that calculates the absolute free energies of biomacromolecules in solution. The free energy difference between different states of the

Tim9–Tim10 complex was estimated by the MM–GBSA method[21] implemented in AMBER9. The MM–GBSA free energy is obtained from a combination of the "gas phase" molecular mechanics energy term, the solvation free energy term and the solute entropy term.

$$G_{\mathrm{mol}} = E_{\mathrm{MM}} + G_{\mathrm{solvation}} - \mathrm{TS}_{\mathrm{solute}},$$

where $E_{\mathrm{MM}} = E_{\mathrm{ele}} + E_{\mathrm{vdw}} + E_{\mathrm{int}}$ and $G_{\mathrm{solvation}} = G_{\mathrm{polar}} + G_{\mathrm{nonpolar}}$. E_{MM} is the "gas phase" molecular mechanical energy, which has contribution from Coulomb electrostatic interactions (E_{ele}), van der Waals interactions (E_{vdw}), and internal degrees of freedom, such as bonds, angles, and dihedral angles (E_{int}). The solvation free energy term $G_{\mathrm{solvation}}$ from continuum electrostatic calculations (the GB solvent model in this case) arises due to the exposure/enclosure of the charged residues (G_{polar}) and a nonpolar solvation term G_{nonpolar} which is hydrophobic in nature and depends linearly on the solvent-accessible surface area. In this study, we refer to the electrostatic components of the free energy as the sum of $E_{\mathrm{ele}} + G_{\mathrm{polar}}$ and the nonpolar components of the free energy as the sum of $E_{\mathrm{vdw}} + G_{\mathrm{nonpolar}}$. The solute entropy term ($\mathrm{TS}_{\mathrm{solute}}$) is computed by the normal mode analysis as implemented by the NMODE module in AMBER. The MM–GBSA free energy was calculated at 300 K based on the first 100 frames and the last 100 frames of the three MD simulation trajectories, respectively, and the difference was extracted for each set of frames.

RESULTS AND DISCUSSION

Thermal dissociation of the Tim9–Tim10 complex

Thermal stability of the Tim9–Tim10 complex was studied by measuring the change of CD intensity at 222 nm. As shown in Figure 2A, although there was a gradual intensity change at temperatures below 40°C and above 60°C, a sharp intensity decrease occurred between 40 and 60°C, showing that the complex was dissociated between 40 and 60°C (not below 40°C) with a melting temperature (T_{m}) at about 50°C. The result of weak dependence at temperatures below 40°C is consistent with the fact that the complex is folded with flexible tentacle-like N- and C-terminals that can undergo conformational change (unfolding) with temperature, and the fact that individual proteins are folded in a molten-globule state.[9,10] Supporting this explanation, similar weak linear temperature dependence was observed for individual unassembled proteins over the whole temperature range of 20–90°C (data not shown).

There is no Trp residue in either Tim9 or Tim10, but one Tyr (Y28) in Tim9 and three Tyr residues (Y41, Y49, and Y69) in Tim10, thus, we studied the thermal dissociation of the complex by following intrinsic Tyr fluorescence (Fig. 2B). In this case, a clear temperature dependence of fluorescence decrease was observed at both low and high temperatures, but not between 40 and 60°C. In contrast, a continuous decrease in fluorescence intensity was observed for Tim10, whereas no clear Tyr fluorescence intensity was detected for Tim9. The same result of T_{m} 51 ± 2°C was obtained for the complex. The result that unassembled proteins would have higher fluorescence intensity than the complex at an identical temperature indicates that at least one Tyr residue is located in a polar environment with its fluorescence (partially) quenched in the complex. Unfortunately, no reliable results could be obtained from near UV CD and DSC studies, due to the low contents of aromatic residues and the dynamic/flexible conformational nature of the complex. Taken together, the far UV CD and fluorescence studies showed that the Tim9–Tim10 complex has a dissociation T_{m} of 51 ± 2°C, and the complex is stable at temperature below 40°C.

Detection of conformational changes in the Tim9–Tim10 complex at physiological temperatures

Because the complex was stable (not dissociated) at temperatures below 40°C, next, we investigated whether a mild temperature increase between 10 and 40°C affects the conformation and/or different types (e.g., electrostatic and hydrophobic) of protein–protein interactions in the complex. To this end, the sensitive stopped-flow fluorescence kinetic method was used.[11,15] Tim9 was mixed with Tim10 at a molar ratio of 1:1, and the Tyr fluorescence intensity change was measured at various temperatures (Fig. 2). As reported before, during the complex formation, the fluorescence intensity increased rapidly at first and followed by a decrease in a slow process (Fig. 2C). The data were analyzed using a single exponential function for the fast (k_{f}) and slow (k_{s}) phase, respectively, and the apparent rate constants (k_{f} and k_{s}) were plotted against temperature (Fig. 2D). Interestingly, although the apparent rate of the fast process (driven by electrostatic interaction) increased with temperature over the whole temperature range, the slow process (hydrophobic packing) presented a bell-shaped curve with a maximum at about 25°C. Thus, the result suggested that there is a conformational change in the complex at physiological temperature, which may be associated with changes in hydrophobic interactions that may be coupled to the formation of a less assembled or exited state of the complex.

To confirm and understand better the temperature-dependent results, we decided to perform the same experiment but using the wild type Tim10 and two single Trp mutants of Tim9, Tim9Y28W, and Tim9F63W, respectively. We have shown that both Trp mutants can form the complex with Tim10 as the wild type protein.[11] Furthermore, the mutant complexes have the same CD spectra as the wild type complex, and the same thermal stability as the wild type complex (data not shown). The

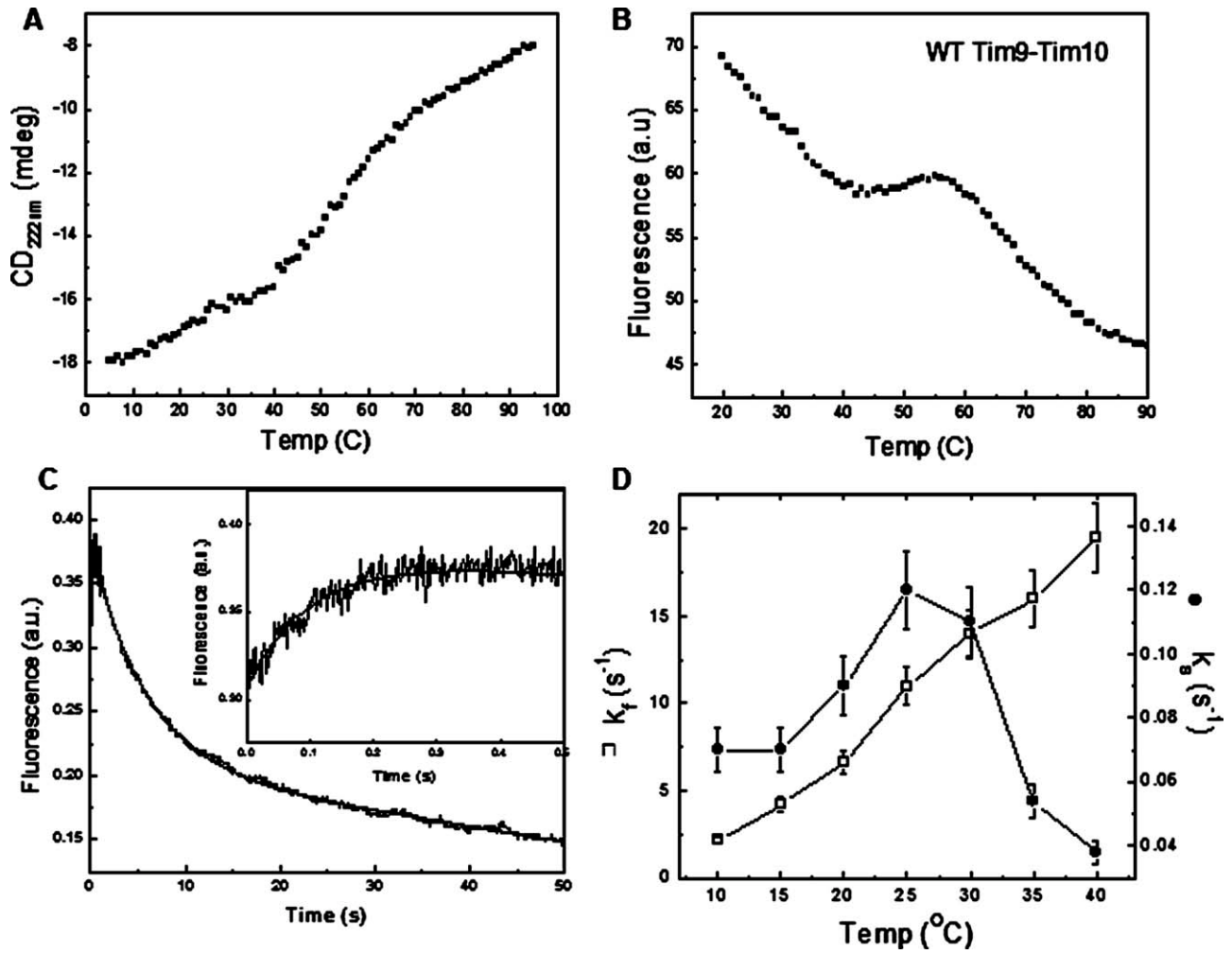

Figure 2

Thermal stability and assembly of the Tim9–Tim10 complex. Thermal denaturation of the complex was measured by following CD intensity change at 222 nm (**A**), and by following Tyr fluorescence (**B**). Temperature was increased at 1°C/min. (**C**) Time course of stopped-flow fluorescence intensity change during the Tim9–Tim10 complex formation, with the fast phase shown in *the inset*. (**D**) Temperature dependence of the fast (open square) and slow (solid circle) rates of the complex formation. The error bars represent the standard errors, $N = 3$.

two mutants had the same overall complex formation kinetics but displayed different sensitivity for the fast and slow kinetic process of complex assembly.[11] Although Tim9Y28W is a good probe for study the fast assembly process, Tim9F63W is sensitive to the slow assembly process.

As controls, Tim9Y28W and Tim9F63W were first mixed with the wild type Tim9 using the stopped-flow method, and Trp fluorescence intensity changes were measured (Fig. 3A,D). Then, the same experiment was performed with Tim10 instead of the wild type Tim9. Whereas large fluorescence intensity changes were observed for the reactions with Tim10, no intensity change was observed for the Tim9 mutants mixed with the wild type Tim9. These results confirm that the observed fluorescence intensity changes were corresponding to the process of complex formation. Next, the temperature dependence of the complex formation was studied by measuring the Trp fluorescence intensity change at temperatures from 5°C to 44°C (Fig. 3B,E). For the Tim9Y28W–Tim10 complex, the data were analyzed using a single exponential function as described previously,[15,22,23] and the apparent rate constants (k_f) were plotted against temperature (Fig. 3C). The rate constants of the fast process of the assembly increased with temperature exponentially, consistent with the same phase of the wild type complex. Moreover, a linear temperature dependence (ln k_f vs. $1/T$) was obtained as analyzed using the Arrhenius equation [Eq. (1) and Fig. 3C inset], where E_a is the activation energy and A is

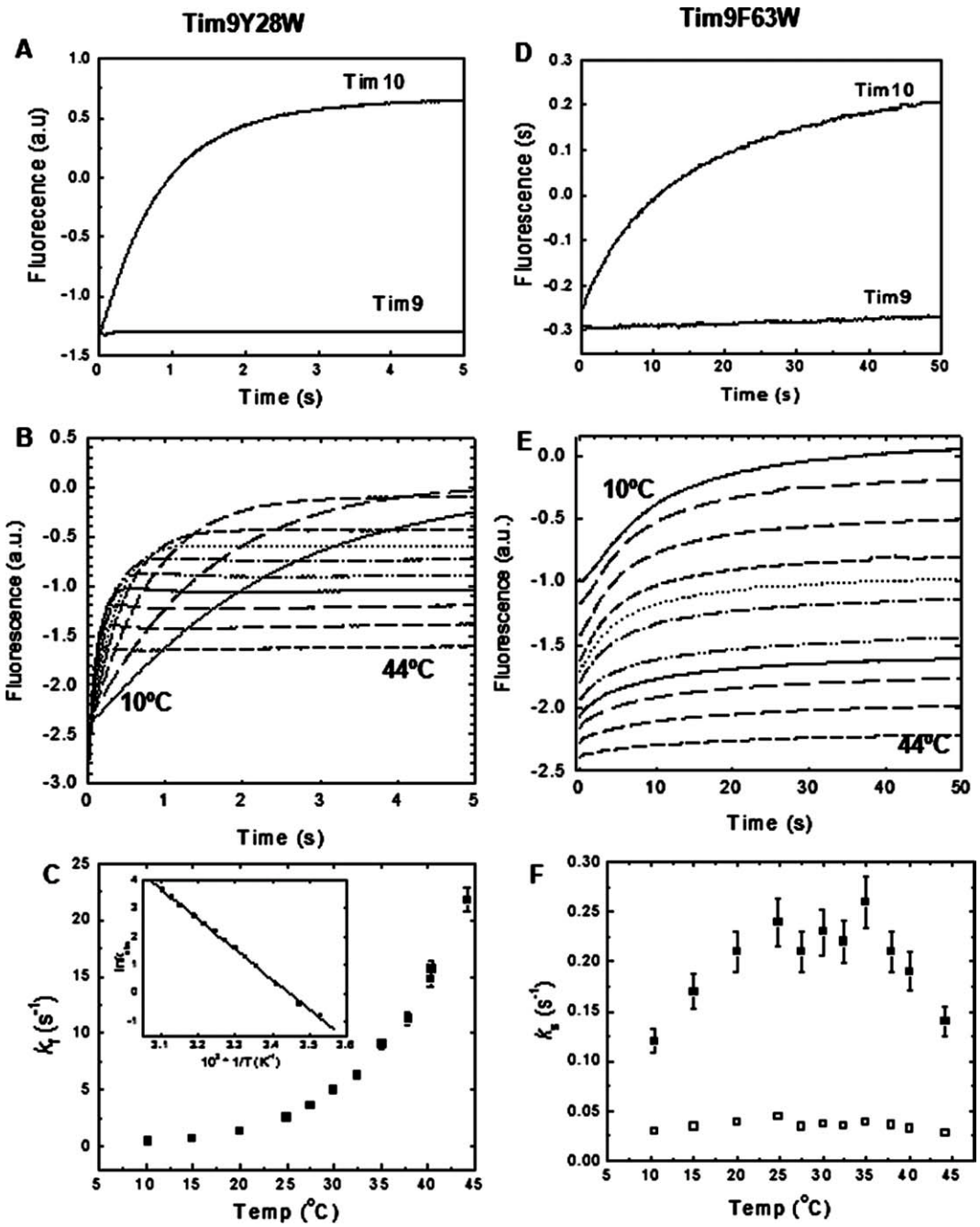

Figure 3

Temperature dependence of assembly of the mutant complexes measured by stopped-flow Trp fluorescence. (**A**) Time courses of fluorescence intensity change after mixing Tim9Y28W with the WT Tim9 or Tim10. (**B**) Time courses of Tim9Y28W–Tim10 complex formation at a temperature from 10°C to 44°C (curves: from bottom to top), respectively. (**C**) Temperature dependence of the rate constants obtained from the curves in (B) using a single exponential function; the inset is Arrhenius plot of the rate constants. (**D**) Time courses of fluorescence intensity change after mixing Tim9F63W with the WT Tim9 or Tim10. (**E**) Time courses of Tim9F63W–Tim10 complex formation at various temperature from10°C to 44°C (from top to bottom). (**F**) Temperature dependence of the rate constants obtained from the curves in (E) using a double exponential function. The error bars represent standard errors, $N = 3$.

a reaction-specific constant, which resulted in the activation energy of 95 kJ M^{-1}. This result suggests that the early process of Tim9–Tim10 assembly is mainly enthalpy driven. In agreement with this the two proteins have opposite net charges at the experimental condition, with Tim9 negatively charged and Tim10 positively charged. It is consistent with our previous findings, based on pH and salt effect on the complex formation, that the early

assembly steps are driven by electrostatic interactions,[15] and also with the observation that electrostatic interactions for polyelectrolyte complexation in high dielectric solutions have large enthalpic components.[24]

$$\ln k_{obs} = -\frac{E_a}{R}\frac{1}{T} + \ln A \quad (1)$$

In contrast with Tim9Y28W–Tim10, the assembly of Tim9F63W–Tim10 complex shows non-Arrhenius behavior (Fig. 3F). In this case, the data were best fit by a double exponential function, where the two observed rate constants correspond to the assembly of the C-terminal helices and/or overall packing or rearrangement of the complex.[11] The apparent rate constants (k_s) were plotted against temperature showing a bell-shaped curve, with an inflection point at about 25°C (Fig. 3F). Because the relative fluorescence intensity change was dominated by the first slow phase (~85%), to diminish the mutual dependencies of the parameters over the temperatures, we also analyzed the data using a single exponential function, and the same bell-shaped curve was obtained (data not shown). Thus, consistent with the slow process of the formation of the wild type complex (Fig. 2D), the result of Tim9F63W–Tim10 complex formation confirms that the slow process exhibits non-Arrhenius behavior with a curvature at about 25°C. Thus the apparent nonlinear temperature dependence of log(k_s) indicates that the slow phase during the assembly of the complex is accompanied by a heat capacity change, and hence a conformational change in the complex. Because the slow phase has been shown to be dominated by formation of the hydrophobic interactions in our previous study,[15] this observed conformational change at about 25°C is most likely hydrophobic in nature.

Furthermore, it has been shown that large-scale protein conformational changes, such as folding and unfolding are usually accompanied by a change in its measured heat capacity. This heat capacity change (ΔC_p) could be attributed to that the nonpolar groups of the protein that are buried in the native state become solvent exposed in the unfolded state.[23,25–28] This exposure of nonpolar residues is coupled to hydration, a major contributor to the heat capacity changes on protein unfolding, which account for the heat capacity changes for many proteins, and correlates well with the surface area of nonpolar groups exposed on unfolding.[29,25] We infer therefore that the conformational change of the Tim9–Tim10 complex we detected at about 25°C indicate a conformational state where the hydrophobic residues become more solvent exposed above 25°C, thus reduces the hydrophobic packing in the complex—an "excited state" of the complex.

The Tim9–Tim10 complex shares structural similarity with the membranes in that most of its hydrophobic residues are packed between the inner and outer layers. Interestingly, a similar bell-shaped temperature dependence was also reported for the assembly of membranes, where the heat capacity changes have been attributed to the transformation of the internal core.[30] At low temperature, movement of the internal hydrophobic core of the membrane bilayer is restricted and results in an ordered liquid crystalline state. On heating the crystalline phase is transformed into a gel state in which molecules attain a higher lateral mobility.

In short, in the present study a bell-shaped temperature dependence was observed for the slow assembly process of the complex, showing that it is accompanied by a heat capacity change and thus the configurational freedom gain by the complex is associated mainly with hydrophobic interactions.[15] Taken together, our experimental results suggest that different conformational complex states exist at physiological temperatures, and the difference between these states is associated with hydrophobic interactions in the complex.

Next, to obtain alternative evidence that physical properties of the Tim9–Tim10 complex changes at physiological temperature, a SPR technique (Biacore) was used. It can measure both association and dissociation of protein complexes, and thus the relative stability of the interactions at various temperatures. As shown in Figure 4A, the relative response (reflectivity) of Tim9 binding to immobilized Tim10 initially increased empirically with temperature followed by a decrease at temperatures above 30°C. Because many other factors may contribute to the response, such as the amount and stability of peptide on the chip that may be affected by temperature, we analyzed the data using the ratios between rates of binding and release at the same temperature. An initial rate method was used, because the Tim9–Tim10 assembly is a multiphase kinetic process. The ratio between the initial velocity of binding (V_{on}) and the initial velocity of release (V_{off}) was plotted against temperature (Fig. 4B). A parabolic shape with a turn point at about 25–30°C was obtained, similar to that of the stopped-flow studies. Because the ratio, V_{on}/V_{off}, is proportional to the binding constant, this result suggested that there was a change in the stability of Tim9–Tim10 interactions at 25–30°C.

In summary, these temperature-dependent results suggest the presence of at least two conformational states of the Tim9–Tim10 complex. They differ in terms of heat capacity and hydrophobic interactions. The conformational change occurred at physiological temperatures, suggesting it may be functionally important.

The conformational change of the Tim9–Tim10 complex correlates with its function

The Tim9–Tim10 complex plays an essential chaperone-like role during import of mitochondrial membrane proteins. The AAC of mitochondrial inner membrane is a physiological substrate of the Tim9–Tim10 complex

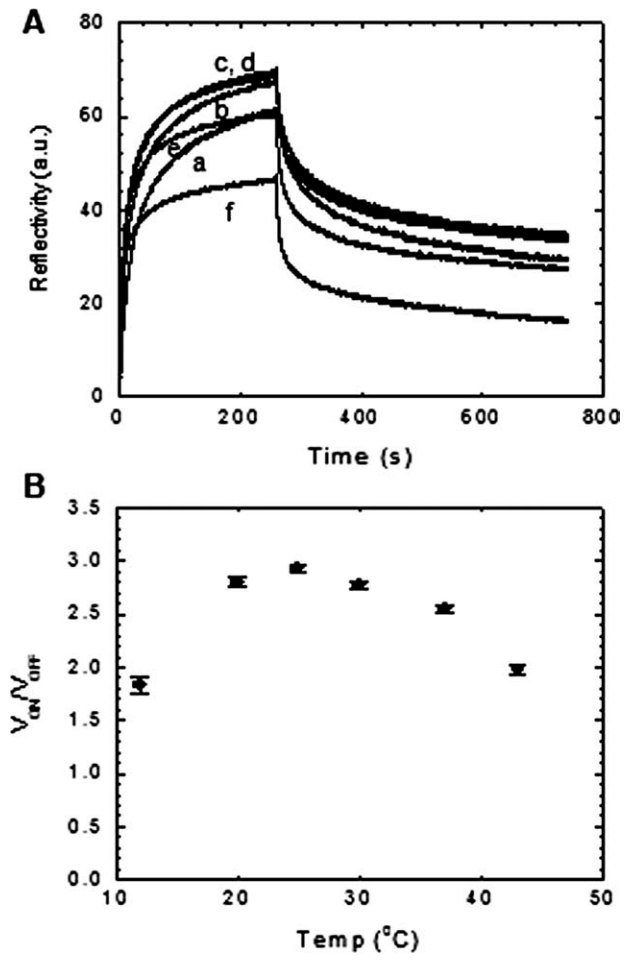

Figure 4

Temperature dependence of Tim9–Tim10 interactions studied using Biacore. (**A**) Time courses of the complex association and dissociation at various temperatures from 12 to 43°C. Curves a–f corresponding to 12, 20, 25, 30, 37, and 43°C, respectively. (**B**) The ratios of velocities V_{on}/V_{off} plotted against temperature. The error bars represent standard errors, $N = 3$.

and has been used extensively in mitochondrial import studies.[31] AAC contains six transmembrane helices forming three internal repeats. Peptide spot array coupled with western blotting studies have shown that the Tim9–Tim10 complex can bind to the hydrophobic transmembrane segments of AAC.[32–34] To understand whether the observed heat capacity change has an effect on the function of the complex, temperature dependence of substrate binding to the Tim9–Tim10 complex was investigated using a peptide derived from the TM3 of AAC.

First, substrate binding to the Tim9–Tim10 complex was studied using stopped-flow Trp fluorescence method. The wild type Tim9–Tim10 complex (containing no Trp residue) was mixed with TM3 (containing a Trp) at various temperatures (Fig. 5A). Although no fluorescence intensity changes were observed for Tim9–Tim10 or TM3 mixed with buffer, clear fluorescence intensity changes were observed on mixing of the Tim9–Tim10 complex and TM3 (Fig. 5A). The data were analyzed with a single

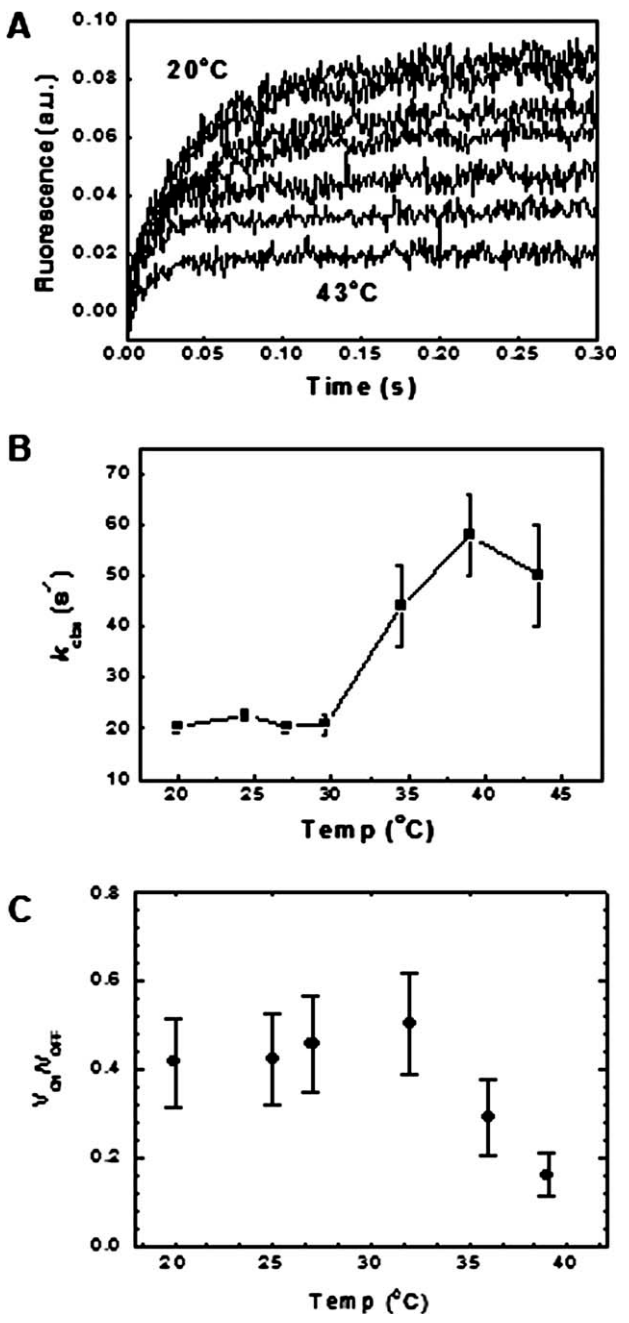

Figure 5

Temperature dependence of substrate binding by the Tim9–Tim10 complex. (**A**) Time courses of Trp fluorescence during the binding of TM3 peptide to the Tim9–Tim10 complex at various temperatures. The reaction was initiated and measured using stopped-flow fluorescence technique at a molar ratio of 1:1. (**B**) Temperature dependence of the observed rate constants of the reactions shown in (A). (**C**) Temperature dependence of TM3 binding of the complex measured using Biacore. The ratio of the initial velocities V_{on}/V_{off} was plotted against temperature. The error bars represent standard errors, $N = 3$.

exponential function and the observed rate constants are shown in Figure 5B. It shows that the observed rate of substrate binding seems independent of temperature below 30°C, but it increases with temperature from 30°C. This inflection temperature is similar to that of the heat capacity change of the Tim9–Tim10 complex, suggesting that the heat capacity change (associated with the rupture of hydrophobic interactions in the Tim9–Tim10 complex) allows the complex to bind its substrate more rapidly.

Next, we asked how temperature affects the stability of substrate binding by the Tim9–Tim10 complex. To address this question, N-terminal biotinylated TM3 was immobilized on a Biacore SA chip and the Tim9–Tim10 complex was injected at various temperatures. The data were analyzed using the ratio of V_{on}/V_{off} as described above and shown in Figure 5C. Although again no obvious difference was observed at temperatures below 30°C, the relative stability of the substrate binding decreased at temperatures above 30°C. This result suggests that although the less assembled E state of the complex can capture its substrate efficiently, it cannot hold substrate tightly, at least for the peptide binding.

Interestingly, the rate of substrate binding has no obvious dependence on temperature below 30°C. It suggests that the activation energy is very low or close to zero, there are a similar number of bonds formed and broken in the transition state, and the process is entropy driven. Furthermore, above 30°C, although the substrate binding rate increased, the strength of the binding decreased due to a stronger temperature dependence of V_{off} than V_{on}. Moreover, the substrate binding is most stable at about 30°C, the optimal temperature for yeast growth. Alternatively, the result may indicate that a stable binding requires complementary interactions between the complex and the full length of the substrate, and/or may reflect the fact that the chaperone function of the complex is to bind substrate transiently during substrate translocation from the outer membrane to the inner membrane. It is worth mentioning that both the Biacore binding and release data cannot be fitted to a single exponential function, suggesting that there is more than one binding site (as expected) on the complex. Unfortunately, how many of the substrate molecules per complex can bind cannot be determined due to the insoluble nature of the hydrophobic transmembrane peptide. Nevertheless and more importantly, the substrate binding studies showed a good temperature correlation between the heat capacity change in the complex and its chaperone function (substrate binding), therefore the subtle conformational change dominated by hydrophobic effects at 25–30°C plays an important role in mediating the function of the Tim9–Tim10 complex.

MD simulations reveal the presence of a slightly unfolded complex

Protein folding/unfolding typically occurs on a time scale beyond the capability of current computational resource. The direct simulation of protein unfolding in a full atomic, explicit solvation and normal physiological condition remains challenging and has only been applied to small systems. A typical computational approach is to employ elevated temperatures to induce the unfolding process.[35,36] The unfolding pathways generated through elevelated simulation temperatures have been compared with experimental data for several proteins.[35,37–39] In general, protein unfolding is essentially independent of simulation temperature, that is, the elevated temperature acts as a "catalyst" to accelerate the unfolding without altering the unfolding pathway. Therefore, the sequence of structural changes during these simulations reflects the intrinsic stability of the studied protein. To study the effect of temperature on the Tim9–Tim10 complex at atomic level, 1 ns MD simulations were performed at 300 K as a benchmark of the native state, at 400 K to resemble the moderate increase of temperature in the experimental methods, and at 450 K aiming to dissociate the complex (Fig. 6). The main chain Cα root-mean-square deviations (RMSDs) at 300 K indicate that the structure of the complex is stable within the 1 ns of simulation (RMSDs below 2 Å; Fig. 6A). At the 400 K, the Cα RMSDs gradually increase to ~5 Å toward the end of the trajectory, showing that the overall structure of the complex is slightly perturbed by the increase of temperature but has not unfolded nor dissociated (Fig. 6A,C). At 450 K, the Cα RMSDs at the end of the simulation increase to ~16 Å, indicating substantial unfolding and dissociation of the complex. The plot of the Cα root-mean-square fluctuations (RMSFs) of individual residues over the simulation time showed that the N- and C-terminal tentacle regions of the complex exhibit higher flexibility than the main helical regions of the complex. On increase of temperature, mobility of the whole complex increased, as seen by the higher RMSFs for all Cα atoms across the complex, and the increase is particularly pronounced in the tentacle regions (Fig. 6B,C). This result is consistent with the experimental observation and suggests that the gradual CD intensity decreases at low tempterature is due to the increase of mobility in the N- and C-tentacle regions.

In summary, through performing MD simulations at a slightly elevated temeperature of 400 K, we generate a set of structures of the Tim9–Tim10 complex that may resemble the E state or a less stable complex state in terms of the enhanced overall motions and the increasingly mobile tentacles of the complex while the overall fold of the complex is intact.

Free energy calculation indicates that the conformational change is driven by hydrophobic interactions

The MM–GBSA method has been applied in studying protein unfolding,[40] protein–protein interactions,[41] and

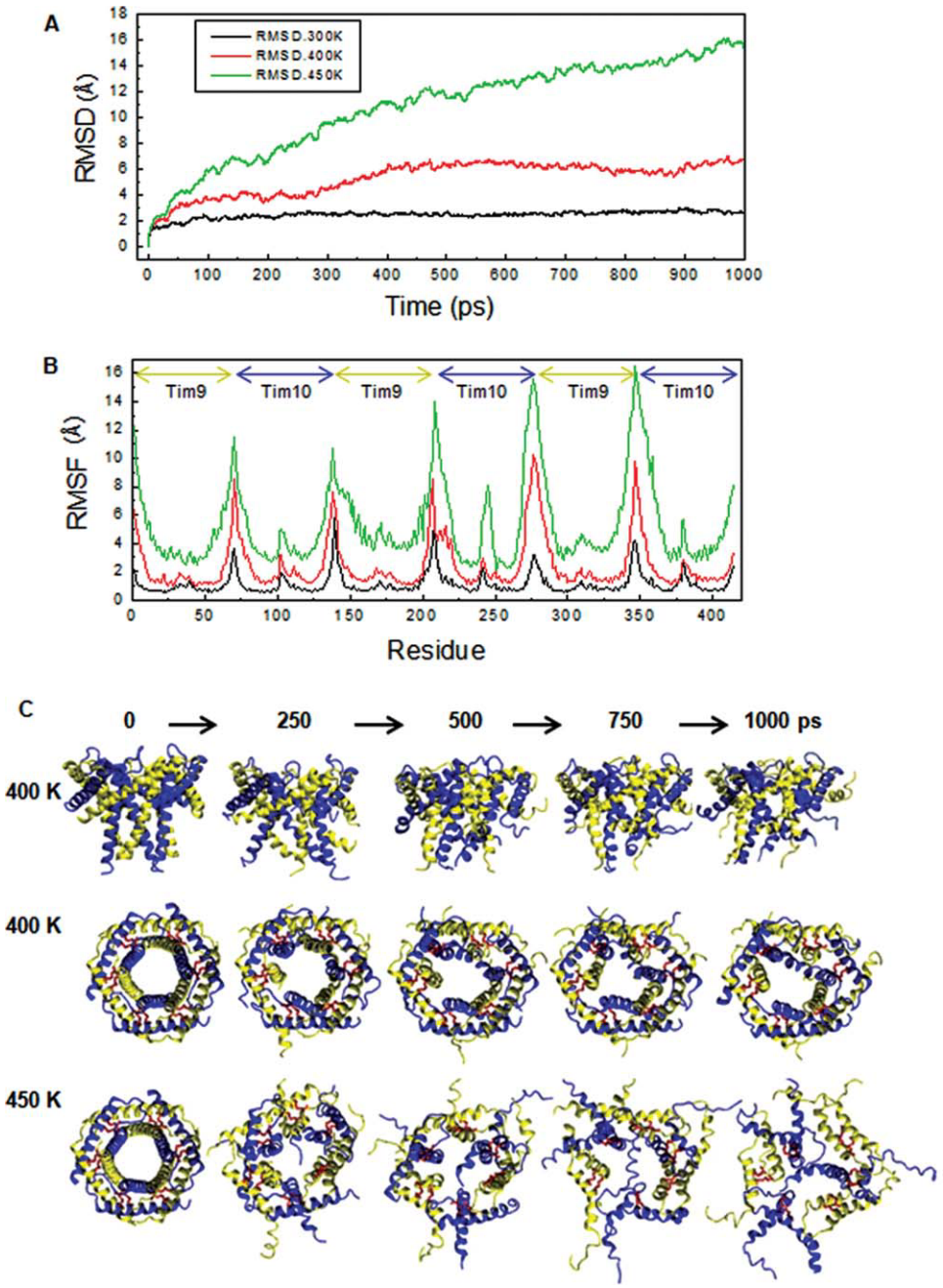

Figure 6

Molecular dynamic simulations of the Tim9–Tim10 complex at various temperatures. (**A**) Cα RMSDs and (**B**) RMSFs of individual residues of the trajectories of 300 K (blue line), 400 K (red line), and 450 K (green line) simulations. (**C**) Structure of the Tim9–Tim10 complex along the simulation at 400 K (1st and 2nd rows) and 450 K (3rd row) with sideview (1st row) and topview (2nd nd 3rd rows). Tim9 is shown in yellow ribbon, Tim10 in blue ribbon, and the disulphide bond between Cys residues in red sticks.

to estimate binding affinities of small molecules to protein.[42] Although it is generally accepted that this method does not tend to replicate the experimentally determined free energy in absolute terms, it has been shown that this method provides a good indication of the trend between changes in the energy terms and experimental data.

To examine the role the hydrophobic interactions in stabilizing the complex, each component of the MM–GBSA free energy was first decomposed into the contribution of each individual residues and the contribution from the hydrophobic residues (Val, Ile, Leu, Met, Phe, Trp, Tyr, and Cys; Fig. 7 and Supporting Information Ta-

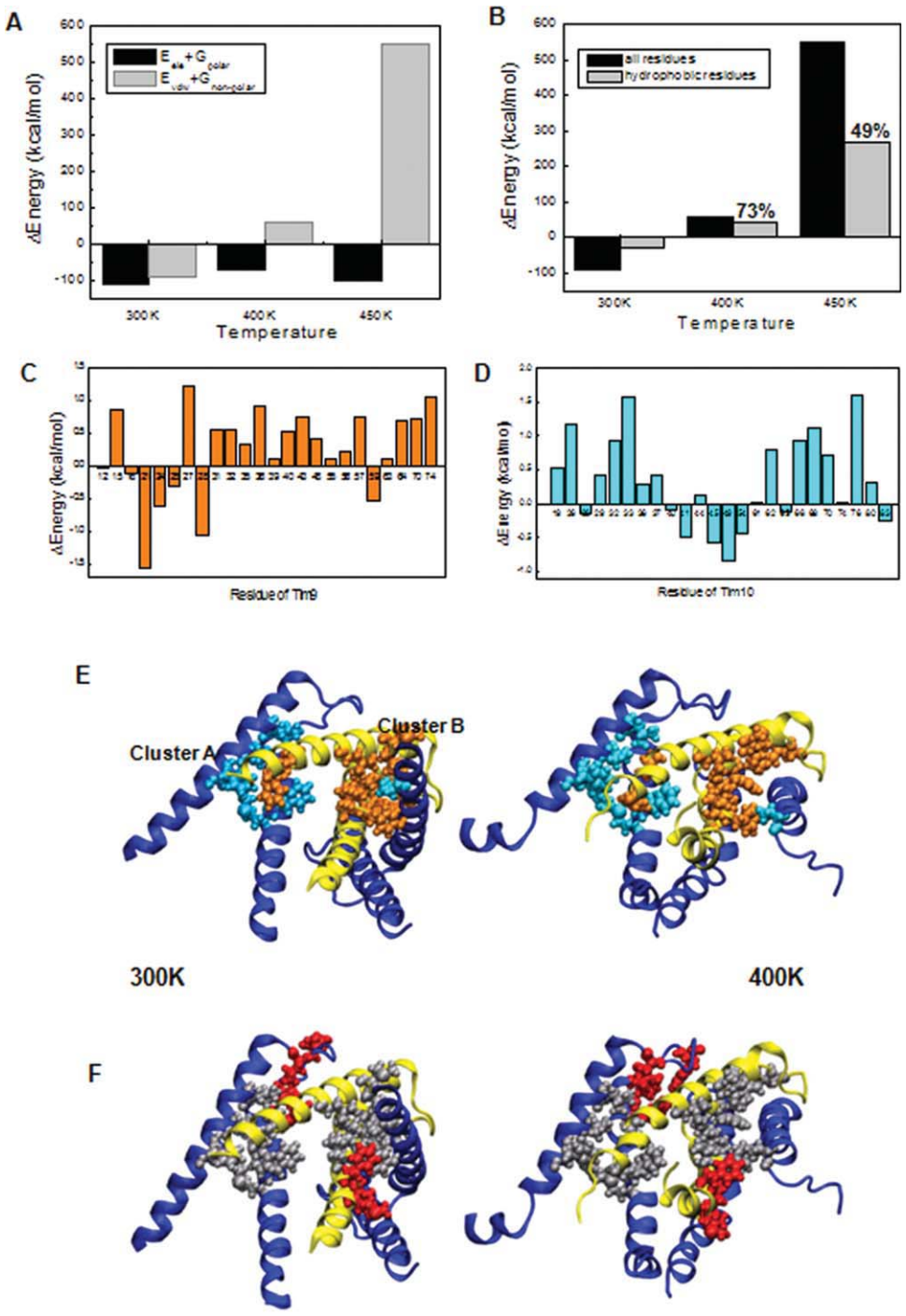

Figure 7

The MM–GBSA free energy change at variouse temperatures. (**A**) The hydrophobic and electrostatic components of the energy change calculated based on the differences between the first 100 frames and the last 100 frames of the MD simulation trajectories. (**B**) The hydrophobic components of the energy change, $\Delta(E_{vdw} + G_{nonpolar})$ for all 414 residues and for the 144 hydrophobic residues (Val, Ile, Leu, Met, Phe, Tyr, and Cys) in the Tim9–Tim10 complex (PDB: 3DXR). $\Delta(E_{vdw} + G_{nonpolar})$ of individual hydrophobic residues of Tim9 (**C**) and Tim10 (**D**). The value displayed for each residue is the average over the three same molecules within the complex. (**E**) The two key hydrophobic clusters formed in the Tim9–Tim10 complex as identified by the energy decomposition analysis. On the left is the native state at 300 K, and on the right is a snapshot taken from the end of the 400 K simulation. Cluster A involves Val70(59), Phe74(63) of TIM9 and Met32(87), Phe33(88), Leu62(117), Val66(121), Tyr69(124), and Phe70(125) of Tim10. Cluster B lies between Leu27(16), Leu31(20), Val32(21), Phe36(25), Val40(29), Phe43(32), Met57(46), and Leu64(53) of Tim9, and Tyr69(262), Val76(269) of the neighboring Tim10. The numbers in the brackets are residue numbers used in the MD simulations as in Figure 6B. (**F**) The stabilizing hydrophobic residues (Met21, Phe24, Met25, and Tyr28 of Tim9 and Tyr41, Ile45, Tyr49 and Leu54 of Tim10) are shown in red together with the residues involved in the clusters A and B in gray.

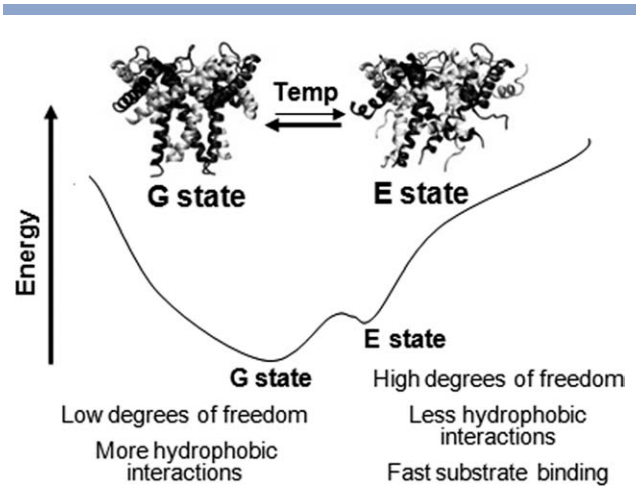

Figure 8

A model for different energy states of the Tim9–Tim10 complex. The ground state (G state) and the excited state (E state) are separated by a low energy barrier. The G state is the highly populated state that contains more hydrophobic interactions and low degrees of freedom, which cannot capture its substrate as efficiently as the low-populated E state. The E state has a relatively high degree of freedom due to disruption of some hydrophobic interactions. This enables the E state to bind substrate more rapidly.

ble 1).[43] The term $\Delta(E_{MM} + G_{solvation})$ increases with increasing temperature, indicating the progression of the extent of unfolding at the end of each simulation, consistent with the measurement of Cα RMSDs that reaches ~5 Å and ~16 Å at the end of the 400 K and 450 K simulation, respectively. As shown in Figure 7A, at 300 K, both the hydrophobic and electrostatic components are favorable (negative value). However, although the electrostatic component still contributes favorably at 400 K and 450 K, the hydrophobic component becomes slightly unfavorable (positive value) at 400 K and significantly unfavorable at 450 K. Thus, the hydrophobic component of the MM–GBSA free energy is the dominant factor that promotes unstability of the complex and drives its unfolding.

There are 144 hydrophobic residues (Val, Ile, Leu, Met, Phe, Tyr, and Cys) in Tim9 and Tim10—~35% out of the total 414 residues in the crystal structure of the Tim9–Tim10 complex. All of these hydrophobic residues are located at the interface between the two layers of the helices (see Fig. 1). The energy decomposition analysis revealed that the contribution from these hydrophobic residues (~35%) accounted for 73% (40.9 kcal/mol out of 56.3 kcal/mol) of the total hydrophobic effects $\Delta(E_{vdw} + G_{nonpolar})$ at 400 K, and it dropped to ~49% at 450 K (Fig. 7B). Thus, the result confirmed that although a higher temperature (450 K) disrupted interactions from all residues hence resulting in dissociation of the complex, a mild temperature perturbation (400 K) acted mainly on the hydrophobic interactions (Figs. 6C and 7B). Furthermore, the dominant effect under the mild temperature perturbation arises mainly from the change in ΔE_{vdw} (37 kcal/mol), thus the decrease of shape complementarity (measured by the change in ΔE_{vdw}), indicating a conformation change that arises from breaking/loose packing of the hydrophobic residues.

To provide further atomic description of the conformational change, the energy contribution by each individual hydrophobic residues to the hydrophobic effect $\Delta(E_{vdw} + G_{nonpolar})$ was plotted (Fig. 7C,D). By examining the location of these residues that contribute most significantly to the destabilizing hydrophobic effects at lower temperature, two hydrophobic clusters between Tim9 and Tim10 are identified. Cluster A involves Val70, Phe74 of Tim9, and Met32, Phe33, Leu62, Val66, Tyr69, Phe70 of Tim10. Cluster B lies between Leu27, Leu31, Val32, Phe36, Val40, Phe43, Met57, and Leu64 of Tim9, and Val76 of the neigboring Tim10 (Fig. 7E). Other hydrophic residues exhibit a stabilizing effect (Met21, Phe24, Met25, Tyr28 of TIM9 and Tyr41, Ile45, Tyr49, and Leu54 of TIM10; Fig. 7F). Nonetheless, the overall stabilizing effect of these residues is offset by the destabilizing effect from residues in clusters A and B. The results suggest that clusters A and B may contain the key residues providing hydrophobic stability for the G state of the Tim9–Tim10 complex, and together or in part they may play an important role in regulating the function of the complex. More detailed experimental studies are required to test and verifying this prediction in future.

CONCLUSIONS

This study showed that dynamic properties of protein–protein interactions can be studied using stopped-flow technique coupled with temperature-dependent analysis. The presence of a functionally important, excited state under physiological conditions was demonstrated experimentally and through computational analysis. We show that the dynamics of the overall hydrophobic residues of the complex, determined by its conformation, plays an important role in regulating substrate binding by the ATP-independent chaperone, Tim9–Tim10 complex.

On the basis of the results, we propose that a low-populated excited state (E state) of the Tim9–Tim10 complex exists in equilibrium with the stable ground state (G state) at physiological temperatures (Fig. 8). The two states differ in terms of hydrophobic interactions, heat capacity, and intrinsic motion. Although the G state has relatively low degrees of freedom (magnitude and direction of intrinsic motion) and more stable hydrophobic interactions, the E state has more degrees of freedom, less hydrophobic interactions and thus more dynamic conformation, similar to the late kinetic intermediate populated during the assembly of the complex. The G and E states are separated by a low energy barrier as the

equilibrium between the two states can be shifted at physiological temperatures. The E state may also be induced by other mild perturbations, such as on substrate binding and protein–protein interactions. Computational analysis of these structures confirmed that a slightly elevated temperature disrupts mainly hydrophobic interactions and that the less optimal packing of hydrophobic interactions is the dominant factor that promotes instability of the complex and drives formation of an excited state. How substrate is released from the Tim9–Tim10 chaperone is unknown. It may be triggered by high affinity downstream interactions between the substrate and the components of the TIM22 complex of the inner membrane. Identification of the key hydrophobic residues (located in two clusters) in destabilizing the G state of the complex provides important information for future studies to address the functional mechanism of the complex at atomic level.

ACKNOWLEDGMENTS

We are grateful to Michael Grant and Bruce Morgan for helpful comments. HL is a Royal Society University Research Fellow (2003).

REFERENCES

1. Alberts B. The cell as a collection of protein machines: preparing the next generation of molecular biologists. Cell 1998;92:291–294.
2. Nooren IM, Thornton JM. Diversity of protein–protein interactions. EMBO J 2003;22:3486–3492.
3. Robinson CV, Sali A, Baumeister W. The molecular sociology of the cell. Nature 2007;450:973–982.
4. Pfanner N, Geissler A. Versatility of the mitochondrial protein import machinery. Nat Rev Mol Cell Biol 2001;2:339–349.
5. Koehler CM. The small Tim proteins and the twin Cx3C motif. Trends Biochem Sci 2004;29:1–4.
6. Wiedemann N, Pfanner N, Chacinska A. Chaperoning through the mitochondrial intermembrane space. Mol Cell 2006;21:145–148.
7. Young JC, Agashe VR, Siegers K, Hartl FU. Pathways of chaperone-mediated protein folding in the cytosol. Nat Rev Mol Cell Biol 2004;5:781–791.
8. Hartl FU, Hayer-Hartl M. Molecular chaperones in the cytosol: from nascent chain to folded protein. Science 2002;295:1852–1858.
9. Lu H, Golovanov AP, Alcock F, Grossmann JG, Allen S, Lian LY, Tokatlidis K. The structural basis of the TIM10 chaperone assembly. J Biol Chem 2004;279:18959–18966.
10. Lu H, Allen S, Wardleworth L, Savory P, Tokatlidis K. Functional TIM10 chaperone assembly is redox-regulated in vivo. J Biol Chem 2004;279:18952–18958.
11. Ivanova E, Jowitt TA, Lu H. Assembly of the mitochondrial Tim9–Tim10 complex: a multi-step reaction with novel intermediates. J Mol Biol 2008;375:229–239.
12. Allen S, Lu H, Thornton D, Tokatlidis K. Juxtaposition of the two distal CX3C motifs via intrachain disulfide bonding is essential for the folding of Tim10. J Biol Chem 2003;278:38505–38513.
13. Webb CT, Gorman MA, Lazarou M, Ryan MT, Gulbis JM. Crystal structure of the mitochondrial chaperone TIM9.10 reveals a six-bladed alpha-propeller. Mol Cell 2006;21:123–133.
14. Baker MJ, Webb CT, Stroud DA, Palmer CS, Frazier AE, Guiard B, Chacinska A, Gulbis JM, Ryan MT. Structural and functional requirements for activity of the Tim9–Tim10 complex in mitochondrial protein import. Mol Biol Cell 2009;20:769–779.
15. Ivanova E, Lu H. Allosteric and electrostatic protein–protein interactions regulate the assembly of the heterohexameric Tim9–Tim10 complex. J Mol Biol 2008;379:609–616.
16. Lu H, Woodburn J. Zinc binding stabilizes mitochondrial Tim10 in a reduced and import-competent state kinetically. J Mol Biol 2005;353:897–910.
17. Ang SK, Lu H. Deciphering structural and functional roles of individual disulfide bonds of the mitochondrial sulfhydryl oxidase Erv1p. J Biol Chem 2009;284:28754–28761.
18. Case DA, Cheatham TE, III, Darden T, Gohlke H, Luo R, Merz KM, Jr., Onufriev A, Simmerling C, Wang B, Woods RJ. The Amber biomolecular simulation programs. J Comput Chem 2005;26:1668–1688.
19. Duan Y, Wu C, Chowdhury S, Lee MC, Xiong G, Zhang W, Yang R, Cieplak P, Luo R, Lee T, Caldwell J, Wang J, Kollman P. A point-charge force field for molecular mechanics simulations of proteins based on condensed-phase quantum mechanical calculations. J Comput Chem 2003;24:1999–2012.
20. Hawkins GD, Cramer CJ, Truhlar DG. Parametrized models of aqueous free energies of solvation based on pairwise descreening of solute atomic charges from a dielectric medium. J Phys Chem 1996;100:19824–19839.
21. Kollman PA, Massova I, Reyes C, Kuhn B, Huo S, Chong L, Lee M, Lee T, Duan Y, Wang W, Donini O, Cieplak P, Srinivasan J, Case DA, Cheatham TE, III. Calculating structures and free energies of complex molecules: combining molecular mechanics and continuum models. Acc Chem Res 2000;33:889–897.
22. Battistuzzi G, Borsari M, Canters GW, de Waal E, Loschi L, Warmerdam G, Sola M. Enthalpic and entropic contributions to the mutational changes in the reduction potential of azurin. Biochemistry 2001;40:6707–6712.
23. Murphy KP, Privalov PL, Gill SJ. Common features of protein unfolding and dissolution of hydrophobic compounds. Science 1990;247:559–561.
24. Ou Z, Muthukumar M. Entropy and enthalpy of polyelectrolyte complexation: Langevin dynamics simulations. J Chem Phys 2006;124:154902.
25. Privalov PL, Makhatadze GI. Heat capacity of proteins. II. Partial molar heat capacity of the unfolded polypeptide chain of proteins: protein unfolding effects. J Mol Biol 1990;213:385–391.
26. Privalov PL. Cold denaturation of proteins. Crit Rev Biochem Mol Biol 1990;25:281–305.
27. Oliveberg M, Tan YJ, Fersht AR. Negative activation enthalpies in the kinetics of protein folding. Proc Natl Acad Sci U S A 1995;92:8926–8929.
28. Prabhu NV, Sharp KA. Heat capacity in proteins. Annu Rev Phys Chem 2005;56:521–548.
29. Makhatadze GI, Privalov PL. Heat capacity of proteins. I. Partial molar heat capacity of individual amino acid residues in aqueous solution: hydration effect. J Mol Biol 1990;213:375–384.
30. Norde W. Colloids and interfaces in Life science. Weinheim: Willey-VCH Verlag Gmbh & co. Kgaa; 2004. pp 183–212.
31. Neupert W, Herrmann JM. Translocation of proteins into mitochondria. Annu Rev Biochem 2007;76:723–749.
32. Curran SP, Leuenberger D, Oppliger W, Koehler CM. The Tim9p–Tim10p complex binds to the transmembrane domains of the ADP/ATP carrier. EMBO J 2002;21:942–953.
33. Vasiljev A, Ahting U, Nargang FE, Go NE, Habib SJ, Kozany C, Panneels V, Sinning I, Prokisch H, Neupert W, Nussberger S, Rapaport D. Reconstituted TOM core complex and Tim9/Tim10 complex of mitochondria are sufficient for translocation of the ADP/ATP carrier across membranes. Mol Biol Cell 2004;15:1445–1458.
34. Vergnolle MA, Baud C, Golovanov AP, Alcock F, Luciano P, Lian LY, Tokatlidis K. Distinct domains of small Tims involved in subunit interaction and substrate recognition. J Mol Biol 2005;351:839–849.

35. Day R, Daggett V. Direct observation of microscopic reversibility in single-molecule protein folding. J Mol Biol 2007;366: 677–686.
36. Pang J, Allemann RK. Molecular dynamics simulation of thermal unfolding of *Thermotoga maritima* DHFR. Phys Chem Chem Phys 2007;9:711–718.
37. Day R, Bennion BJ, Ham S, Daggett V. Increasing temperature accelerates protein unfolding without changing the pathway of unfolding. J Mol Biol 2002;322:189–203.
38. Ferguson N, Day R, Johnson CM, Allen MD, Daggett V, Fersht AR. Simulation and experiment at high temperatures: ultrafast folding of a thermophilic protein by nucleation-condensation. J Mol Biol 2005;347:855–870.
39. Mayor U, Guydosh NR, Johnson CM, Grossmann JG, Sato S, Jas GS, Freund SM, Alonso DO, Daggett V, Fersht AR. The complete folding pathway of a protein from nanoseconds to microseconds. Nature 2003;421:863–867.
40. Onufriev A, Case DA, Bashford D. Structural details, pathways, and energetics of unfolding apomyoglobin. J Mol Biol 2003;325:555–567.
41. Liang S, Li L, Hsu WL, Pilcher MN, Uversky V, Zhou Y, Dunker AK, Meroueh SO. Exploring the molecular design of protein interaction sites with molecular dynamics simulations and free energy calculations. Biochemistry 2009;48:399–414.
42. Hou T, Wang J, Li Y, Wang W. Assessing the performance of the MM/PBSA and MM/GBSA methods. 1. The accuracy of binding free energy calculations based on molecular dynamics simulations. J Chem Inf Model 2010;51:69–82.
43. Wimley WC, White SH. Experimentally determined hydrophobicity scale for proteins at membrane interfaces. Nat Struct Biol 1996;3:842–848.